Electronic Supplementary Material (ESI) for Chemical Communications.
This journal is © The Royal Society of Chemistry 2022

Electronic Supplementary Information

A water-soluble sensor for distinguishing D_2O from H_2O by dual-channel absorption/fluorescence ratiometry

Fei Zheng,[†] Yanju Luo,*[,†,‡] Chenghui Li,[‡] Yan Huang,[†] Zhiyun Lu,[†] Xiandeng Hou*[,†,‡]

[†]*Key Laboratory of Green Chemistry and Technology (Ministry of Education), College of Chemistry, Chengdu, Sichuan 610064, China. Email: houxd@scu.edu.cn*

[‡] *Analytical & Testing Center, Sichuan University, Chengdu, Sichuan 610064, China. Email: luoyanju@scu.edu.cn*

Table of Contents

1. Experimental Section S4
1.1 Reagents and Methods S4
1.2 Synthesis and Characterization S4
1.2.1 Scheme S1. Synthetic route of **Cy** S6
1.2.2 Scheme S2. Reaction mechanism for the formation of **Cy** S6
1.3 Calculation of the pK_a value S6
1.4 Detection the relative content of H_2O and D_2O S6
1.5 RGB colorimetric S7
1.6 Method reliability S7
2. Supplementary Tables and Figures S8
Figure S1 ^{1}H NMR spectra of **Cy** in DMSO-d_6 .....S8
Figure S2 ^{13}C NMR spectra of **Cy** in DMSO-d_6 .....S8
Figure S3 HRMS spectra of **Cy**. S9
Figure S4 FTIR spectra of **Cy** S9
Table S1 The chemical and physical properties of H_2O and D_2O S10
Figure S5 Optimization diagram of the sensor concentration S11
Figure S6 **Cy** detect D_2O content in H_2O via dual-channels S12
Figure S7 Fluorescence decay curves and FTIR spectra S13
Table S2 The fitted photoluminescence lifetime data of **Cy** S13
Figure S8 The stability of **Cy** S14
Figure S9 The selectivity of **Cy** S15
Figure S10 The selectivity of **Cy** S16
Figure S11 The anti-interference of **Cy** S16
Scheme S3 The basic construction of 3D-printed setup S17
Figure S12 Calibration curve of the RGB S17
Figure S13 The accuracy of **Cy** S18
Table S3 Analytical results for the determination of H_2O content in total volume (%) S18
Table S4 Comparison of currently reported organic small-molecule optical sensors based on the acid-base response mechanism for distinguishing between H_2O and D_2O S19
Table S5 Comparison of currently reported optical sensors for distinguishing between H_2O and D_2O S21

Table S6 Comprehensively analyze the advantages and disadvantages of representative D_2O optical sensors. S22

3. Reference S23

1. Experimental Section

1.1 Reagents and Methods

Unless otherwise described, all reagents and anhydrous solvents used in this work were purchased from commercial sources and used without further purification. D_2O was purchased from Sigma-Aldrich, and dimethyl sulfoxide (DMSO, 99.7%, Superdry, with molecular sieves, J&K Seal), acetonitrile (MeCN, 99.9%, Superdry, with molecular sieves, J&K Seal) and *N*,*N*-dimethylformamide (DMF, 99.8%, Superdry, with molecular sieves, J&K Seal) were purchased from J&K Scientific Co. Ltd. (Beijing, China). 2-((*E*)-2-((*E*)-2-Chloro-3-(2-((*E*)-3,3-dimethyl-1-propylindolin-2-ylidene)ethylidene)cyclohex-1-en-1-yl)vinyl)-3,3-dimethyl-1-propyl-3H-indol-1-ium iodide (IR-780) was purchased from JiangSu Aikon Biomedical R&D Co., Ltd. (Nanjing, China). Resorcinol were purchased from Bide Pharmaceutical Technology Co., Ltd. (Shanghai, China). Deionized water was used to prepare the buffer solutions and as the analyte. For column chromatography, 300−400 mesh silica gel was used to purify the crude product.

^{1}H NMR and ^{13}C NMR spectra were recorded on a Bruker AVANCE II-400 MHz spectrometer at 400 and 100 MHz in DMSO-d_6, respectively. Tetramethylsilane (TMS) was used as an internal standard. All chemical shift data are reported in the standard δ notation of parts per million (ppm). Splitting patterns were designed as follows: s (singlet), d (doublet), t (triplet) and m (multiplet). High-resolution mass spectra (HRMS) were measured on a Q-TOF Premier ESI mass spectrometer. Fourier transform-infrared spectra (FTIR) were measured on a Bruker INVENIO R, and pH values of the samples were measured using a PHS-3E pH meter. UV-visible spectra were measured on a Shimadzu UV-3600 spectrophotometer. Photoluminescence spectra were recorded on a Horiba Jobin Yvon Fluoromax-4 fluorescence spectrophotometer. Transient photoluminescence decay characteristics of the solution samples were recorded on a Single Photon Counting Controller FluoroHub-B (Horiba Jobin Yvon). Photographs were taken using a Huawei Mate20 smartphone.

1.2 Synthesis and Characterization.

Synthesis of (*E*)-2-(2-(6-hydroxy-2,3-dihydro-1H-xanthen-4-yl)vinyl)-3,3-dimethyl-1-propyl-3H-indol-1-ium iodide (**Cy**). Scheme S1 shows the synthetic route for the sensor **Cy**. Under a nitrogen atmosphere, resorcinol (110 mg, 1 mmol) and K_2CO_3 (138 mg, 1 mmol) were added to a two-necked flask containing 5 mL anhydrous acetonitrile, and then the mixtures were stirred at room temperature for 20 min. After that, the acetonitrile solutions of IR-780 (267 mg, 0.2 mmol) were added to the reaction system, and the whole reaction was heated at 50 °C for 4 h. Then the solvent was removed by rotary evaporation, and the residual solid was chromatographed with a silica gel column using dichloromethane/methanol (50/1, *v*/*v*) as an eluent to finally obtain a blue-green powder (yield: 67%).

The reaction mechanism for the synthesis of **Cy** is unique. As shown in Scheme S2, IR-780 and resorcinol under the basic conditions will undergo the straightforward nucleophilic substitution of chlorine atom, retro-Knoevenagel reaction, cyclization reaction and dehydration reaction in sequence,[1] then finally obtain the target compound **Cy**. The molecular structure of the sensor **Cy** was characterized by ^{1}H NMR, ^{13}C NMR spectra, HRMS analyses and FTIR spectra (Figure S1-Figure S4). Due to the efficient hydrogen-deuterium exchange of the phenolic hydroxyl group of **Cy** in the deuterated reagent, the relevant hydrogen signal is indiscernible in the ^{1}H NMR spectrum. Hence, the FTIR spectrum was used for supplementary characterization, and the peak around 3100 cm^{-1} indicates the existence of –OH. ^{1}H NMR (400 MHz, DMSO-d_6) δ (ppm): 8.54 (d, *J* = 14.8 Hz, 1H), 7.75 (d, *J* = 6.0 Hz, 1H), 7.65 (d, *J* = 8.0 Hz, 1H), 7.55 (s, 1H), 7.52 (d, *J* = 8.8 Hz, 1H), 7.48 (d, *J* = 8.4 Hz, 1H), 7.41 (t, *J* = 7.2 Hz, 1H), 6.90 (s, 1H), 6.86 (dd, *J* = 8.4, 2.0 Hz, 1H), 6.49 (d, *J* = 14.8 Hz, 1H), 4.34 (t, *J* = 6.8 Hz, 2H), 2.72 (t, *J* = 5.6 Hz, 2H), 2.67 (t, *J* = 6.0 Hz, 2H), 1.85-1.80 (m, 4H), 1.75 (s, 6H), 0.99 (t, *J* = 7.2Hz, 3H). ^{13}C NMR (100 MHz, DMSO-d_6) δ (ppm): 176.7, 163.3, 161.4, 154.9, 144.3, 142.2, 135.2, 129.8, 129.3, 126.9, 125.8, 123.2, 115.8, 114.9, 114.4, 113.3, 103.6, 102.5, 50.5, 46.3, 28.7, 28.1, 24.1, 21.2, 20.5, 11.5. HRMS (ESI) m/z for $C_{28}H_{30}INO_2$ $(M\text{-}I)^+$ Calcd.: 412.2271, Found: 412.2275.

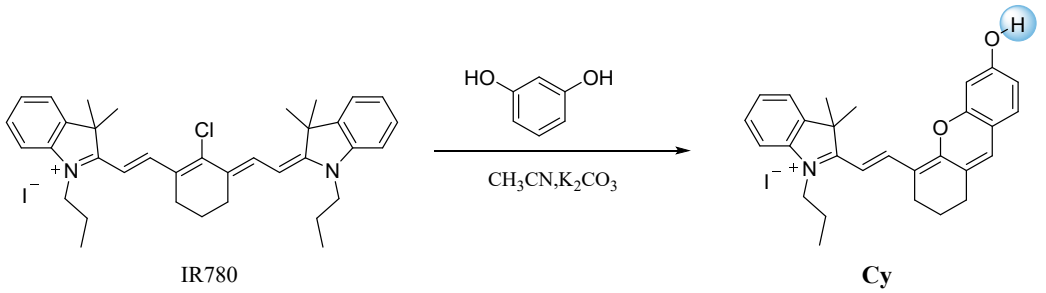

Scheme S1. Synthetic route of **Cy**.

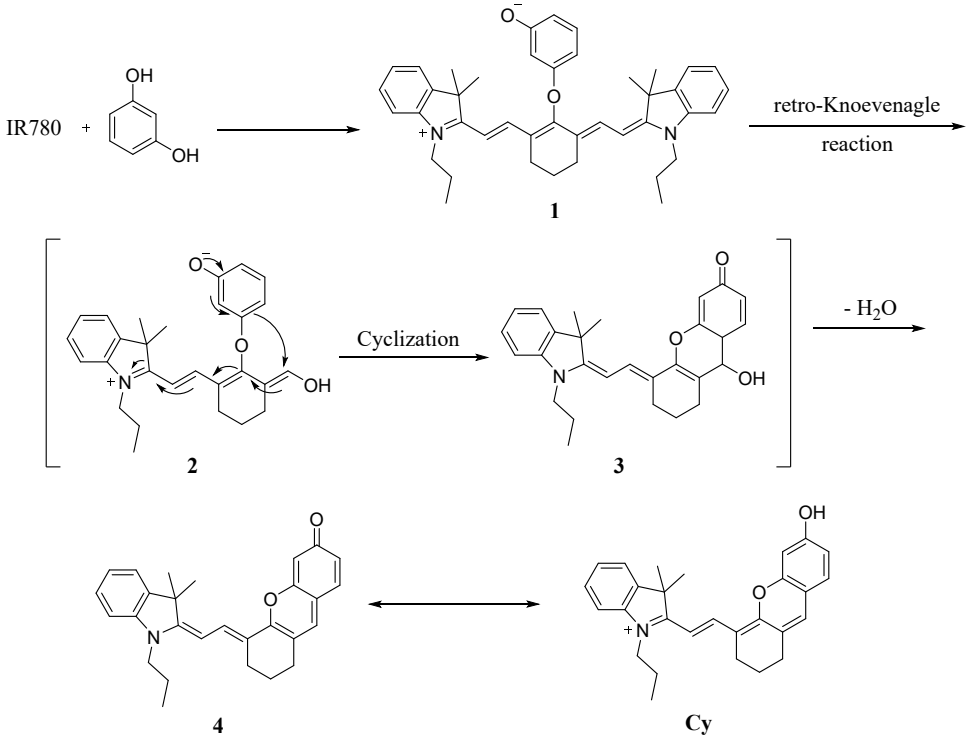

Scheme S2. Reaction mechanism for the formation of **Cy**[1].

1.3 Calculation of the pK_a value

Prepare buffer solutions of the sensor **Cy** with various pH values from 4.01 to 10.02 and characterize the corresponding fluorescence spectra. The pK_a value of **Cy** was calculated by regression analysis of the fluorescence intensity as a function of pH, where the analysis should fit to the Henderson-Hasselbalch-type mass action equation:

$$\log [(F_{max} - F)/(F - F_{min})] = pK_a - pH$$

Where F is the fluorescence emission intensity at 725 nm, F_{max} and F_{min} are the corresponding maximum and minimum limiting values of F, respectively.

1.4 Detection the relative content of H_2O and D_2O

Typically, the stock solution of **Cy** was prepared by dissolving **Cy** in ultra-dry DMF

(2 mM). Then, 22.5 μL **Cy** was added to D_2O (or H_2O or D_2O-H_2O mixtures) and the final concentration of the sensor was 100 μM. UV-vis absorption and fluorescence emission spectra were conducted on the as-prepared solution samples. During the measurements, the lids of the cuvettes are always closed to prevent D_2O from absorbing moisture so as to affect the analytical results. All the experiments were repeated in triplicate to obtain consistent values.

In all subsequent experiments, the concentration of the sensor solution was fixed at 100 μM and the detection system contained 5 vol% DMF.

1.5 RGB colorimetric

The stock solutions of the sensor **Cy** were added to different systems separately, which contained distinct H_2O-D_2O relative content. The detection process is shown in Scheme 2. Pictures of samples were taken with a smartphone and opened with the smartphone analysis application (APP). The detection region was selected in the APP (*Palette Cam*). Generally, the middle part of the reaction solution was selected for sampling. The numerical values of RGB were computed by the APP software and the calibration curve was obtained through data analysis.

1.6 Method reliability

Randomly prepare five samples with various H_2O-D_2O content (unknown relative proportion). The prepared samples were subjected to analysis with FTIR spectra (classical instrumental method) and the proposed **Cy** sensor, including absorption, fluorescence and RGB three channels. The FTIR spectra of all samples were performed on a Bruker INVENIO R Fourier transform-infrared spectrophotometer with the attenuated total reflection (ATR) mode.

2. Supplementary Tables and Figures

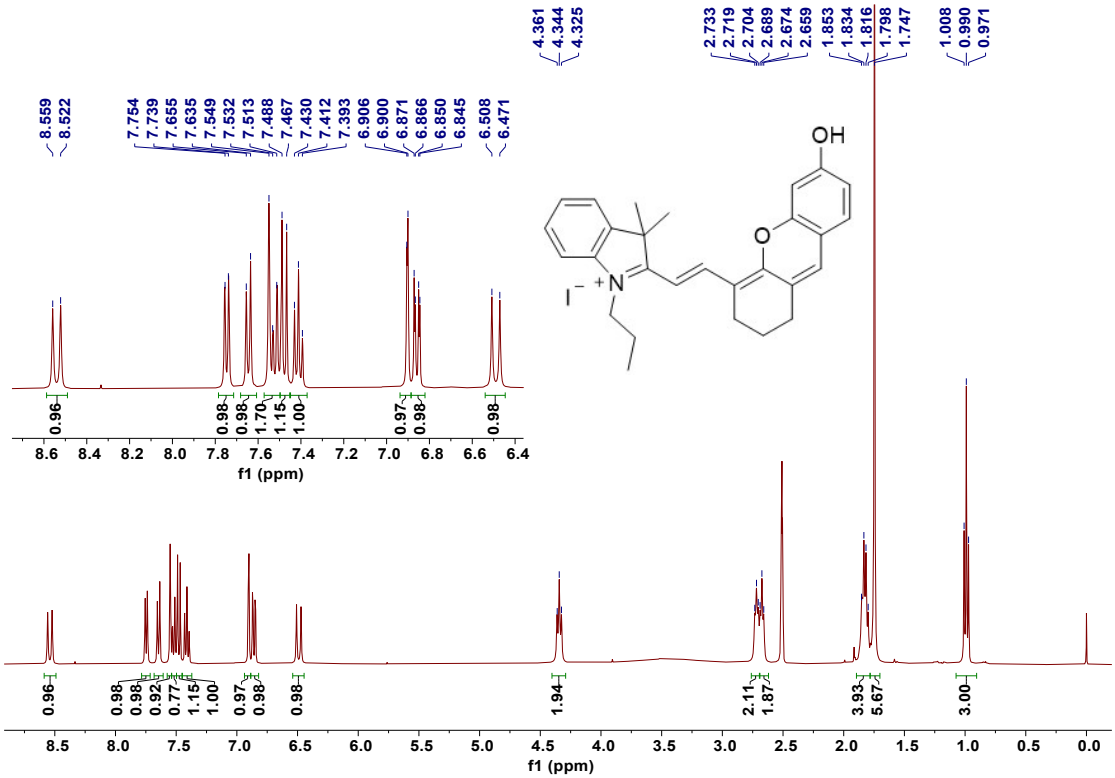

Fig. S1 [1]H NMR spectrum of **Cy** in DMSO-d_6.

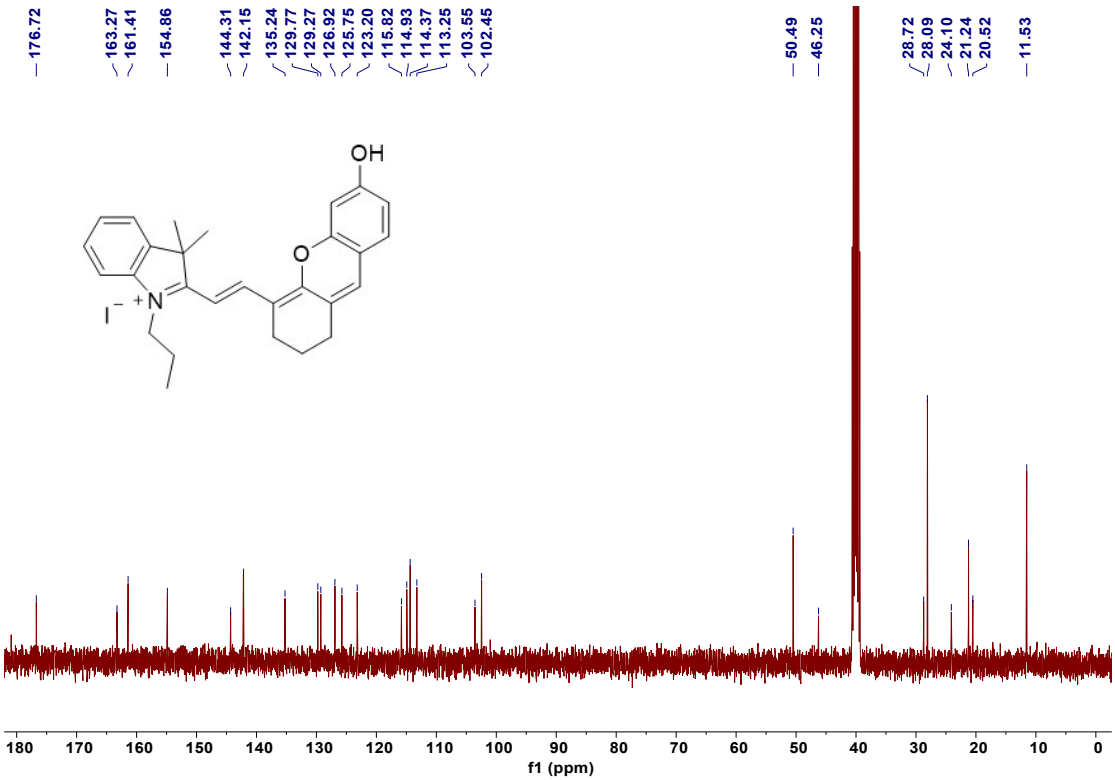

Fig. S2 [13]C NMR spectrum of **Cy** in DMSO-d_6.

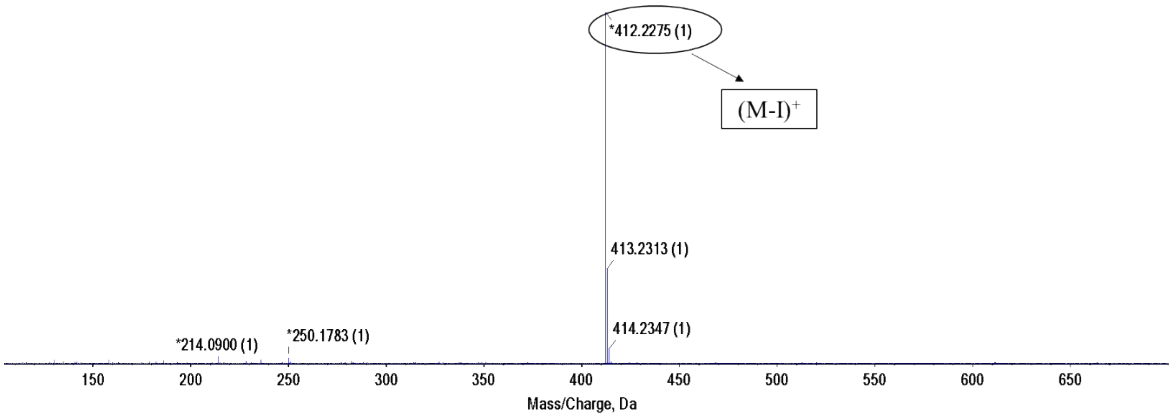

Fig. S3 HRMS spectrum of **Cy**.

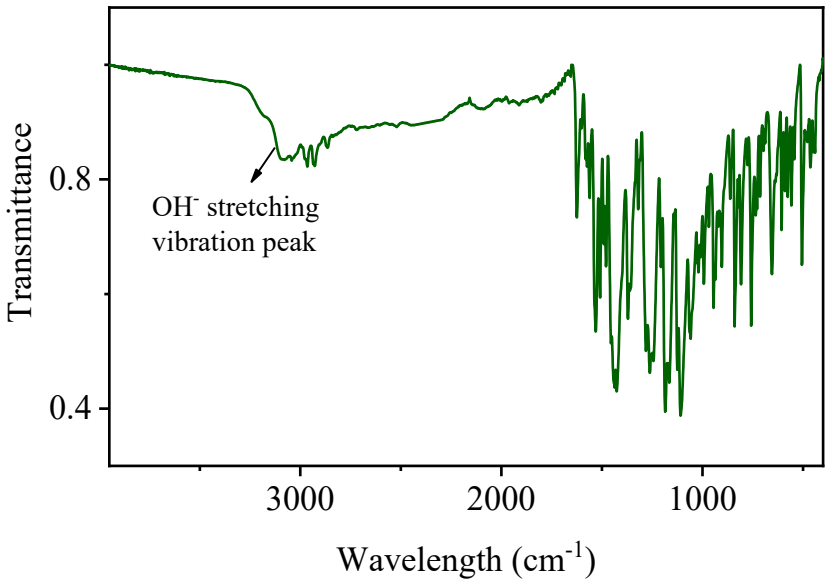

Fig. S4 FTIR spectrum of **Cy**.

Table S1 The chemical and physical properties of H_2O and D_2O

Property	H_2O	D_2O
Melting point / ℃	0.00	3.79
Boiling point / ℃	100	101.4
Relative density / g·mL^{-1} (20 ℃)	0.997	1.108
Heat of evaporation / kJ·mol^{-1}	40.67	41.6
Heat of fusion / kJ·mol^{-1}	6.008	6.276
Freezing point lowered / °C	1.86	2.00
Surface tension (at 25 °C, N·m^{-1})	0.07198	0.07187
Ion product constant (K_w)	1.00×10^{-14}	2.00×10^{-15}
Refractive index (at 20 °C)	1.33298	1.32844
pH	6.4-7.0	7.5

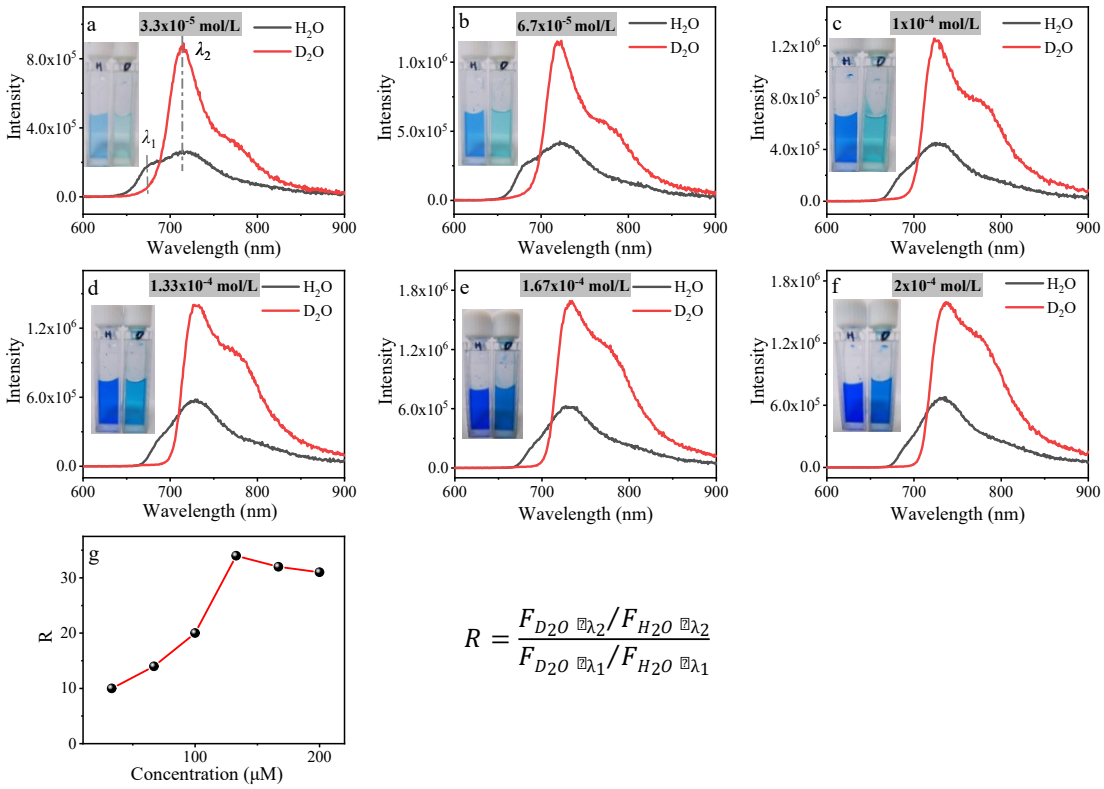

$$R = \frac{F_{D2O\ \lambda_2}/F_{H2O\ \lambda_2}}{F_{D2O\ \lambda_1}/F_{H2O\ \lambda_1}}$$

Fig. S5 The fluorescence spectra of **Cy** in D_2O and H_2O, where the concentration of **Cy** is 3.3 × 10^{-5} mol/L (a), 6.7 × 10^{-5} mol/L (b), 1.0 × 10^{-4} mol/L (c), 1.33 × 10^{-4} mol/L (d), 1.67 × 10^{-4} mol/L (e) and 2.0 × 10^{-4} mol/L (f) respectively (inset: the photos of **Cy** in D_2O and H_2O, respectively). (g) Optimization diagram of the sensor concentration.

In the preliminary experiments, we found that the concentration of **Cy** could affect the output of the ratiometric signal, thus affecting the sensitivity of the sensor. On this basis, we optimized the concentration of **Cy** through comparing the difference of these ratiometric signals between D_2O and H_2O. As shown in **Fig. S5**, when the sensor concentration is 1.33 × 10^{-4} M, the ratio of ratiometric signal (R) reaches the maximum. Nevertheless, considering the effect of naked-eye visualization, we finally chosen the concentration of 1 × 10^{-4} M to realize the good sensitivity and distinct color difference at the same time.

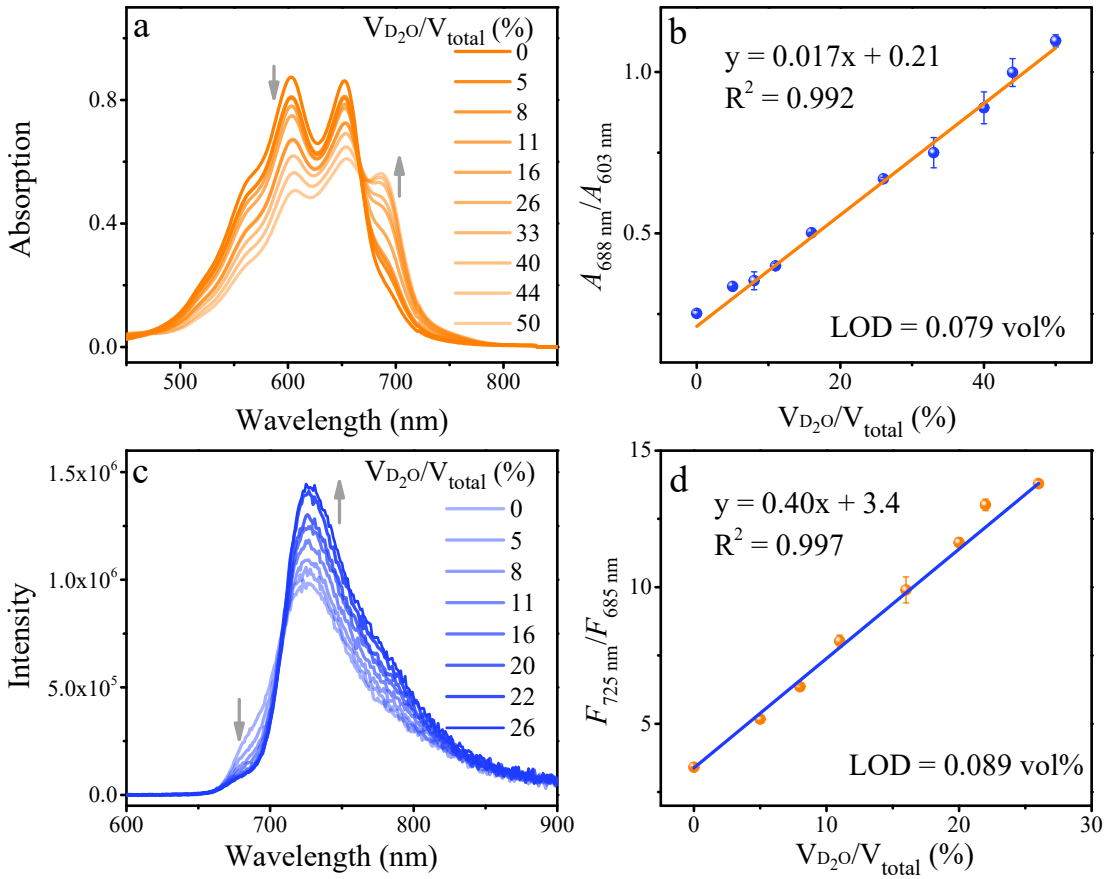

Fig. S6 (a) UV-vis absorption spectra of **Cy** in H_2O-D_2O mixtures with different D_2O fractions (0-50%, v/v). (b) Relationship between A_{688}/A_{603} of **Cy** with D_2O content in total volume. (c) Fluorescence emission spectra of **Cy** in H_2O-D_2O mixtures with different D_2O fractions (0-26%, v/v) (λ_{ex} = 580 nm). (d) Relationship between F_{725}/F_{685} values of **Cy** with D_2O content in total volume ($V_{total} = V_{H_2O} + V_{D_2O}$).

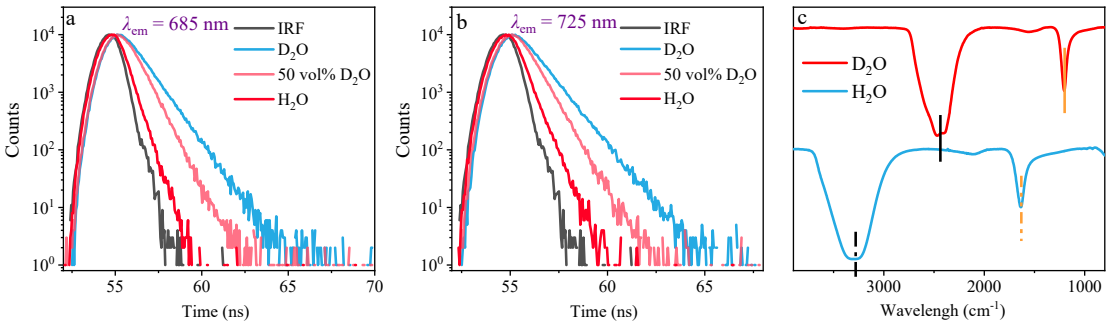

Fig. S7 Fluorescence decay curves of **Cy** in D_2O, H_2O and 50 vol% of D_2O monitored at (a) 685 nm and (b) 725 nm at 298K (λ_{ex} = 590 nm, IRF: Instrument response function). (c) FTIR spectra of pure D_2O and pure H_2O.

Table S2 The fitted photoluminescence lifetime data of **Cy** in D_2O, H_2O and 50 vol% of D_2O at 298 K (λ_{ex} = 590 nm).

	λ_{ex} (nm)	λ_{em} (nm)	Life time (ns)	content (%)	χ^2
D_2O	590	685	τ = 1.01	100	0.95
		725	τ = 0.97	100	0.91
50 vol% D_2O	590	685	τ = 0.73	100	1.02
		725	τ = 0.70	100	0.82
H_2O	590	685	τ = 0.32	100	1.10
		725	τ = 0.35	100	1.20

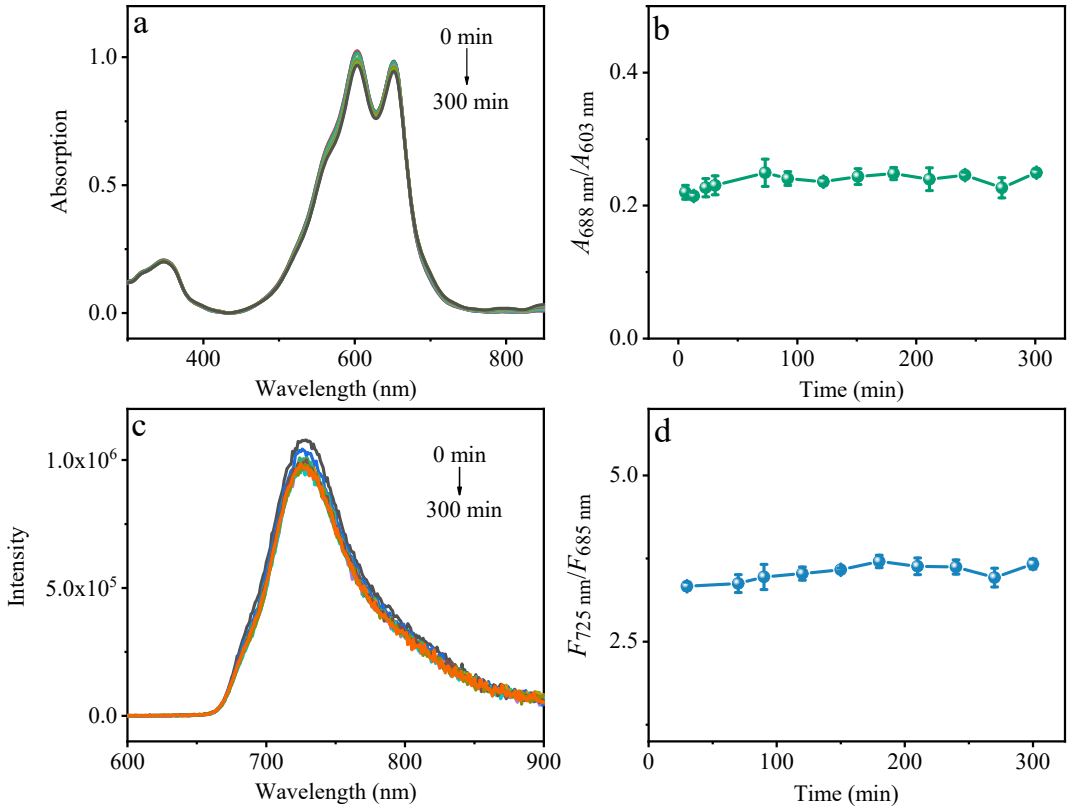

Fig. S8 Time-dependent UV-vis absorption spectra (a) and relationship between A_{688}/A_{603} with time (b) of the sensor **Cy** in H_2O. Time-dependent fluorescence emission spectra (c) and relationship between F_{725}/F_{685} with time (d) of the sensor **Cy** in H_2O (λ_{ex} = 580 nm).

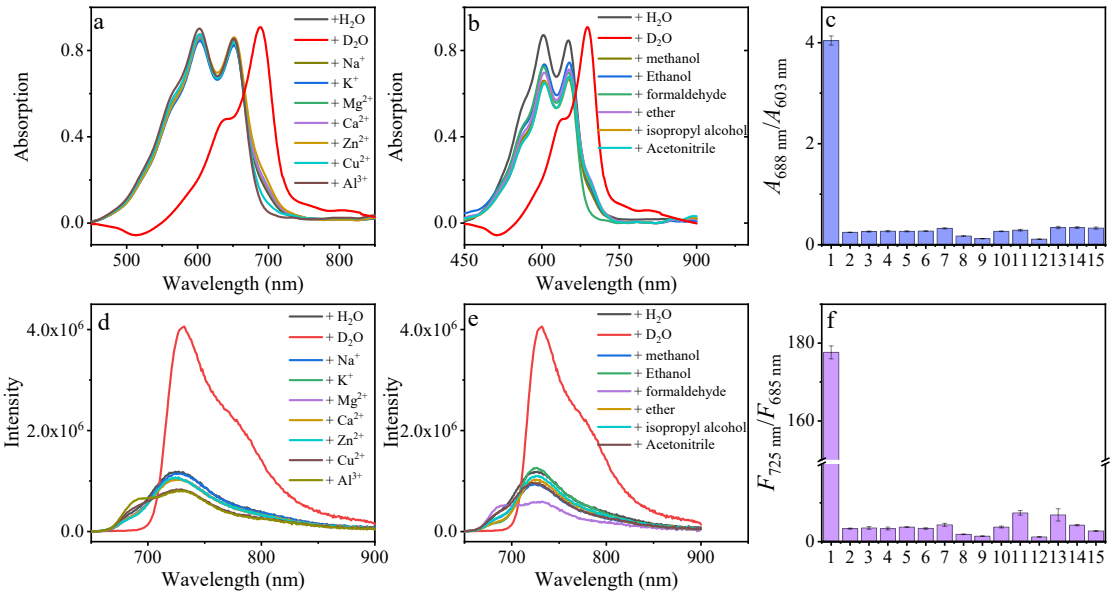

Fig. S9 UV-vis absorption spectra (a) and fluorescence emission spectra (d) of **Cy** in the D_2O, H_2O and H_2O containing various metal ions (concentration: 1 mM; counter ion: Cl^-). UV-vis absorption spectra (b) and fluorescence emission spectra (e) of **Cy** in the D_2O, H_2O and H_2O containing 11 vol% different organic pollutant species. Absorption (c) and fluorescence (f) response of **Cy** in the presence of the other common species. 1, D_2O; 2, H_2O; 3, Na^+; 4, K^+; 5, Mg^{2+}; 6, Ca^{2+}; 7, Zn^{2+}; 8, Cu^{2+}; 9, Al^{3+}; 10, methanol; 11, ethanol; 12, formaldehyde; 13, ether; 14, isopropyl alcohol; and 15, acetonitrile (λ_{ex} = 580 nm).

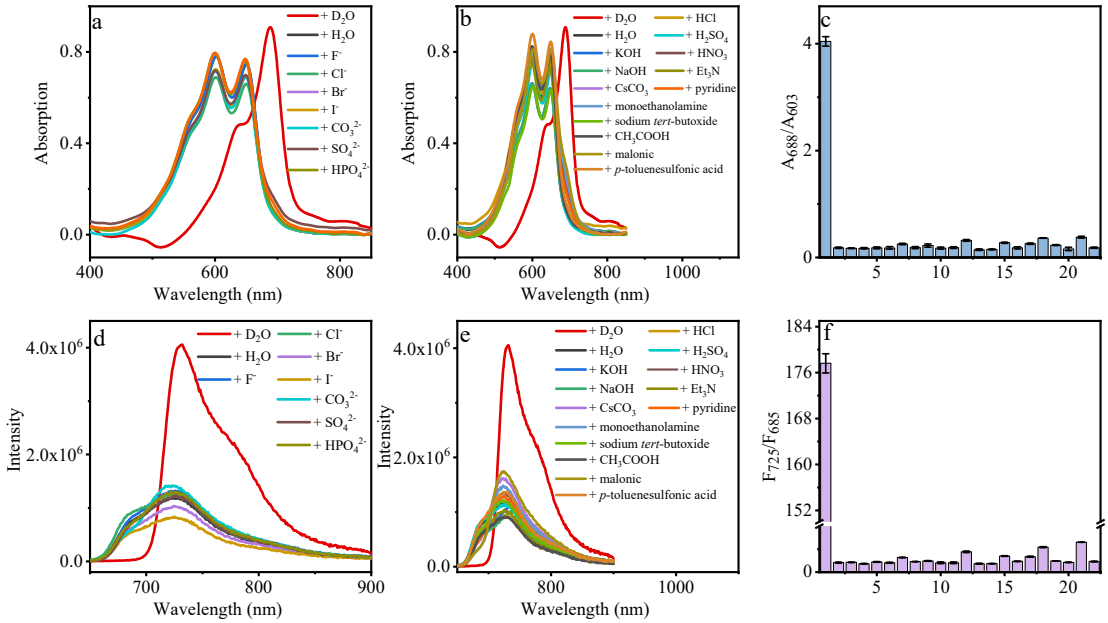

Fig. S10 UV-vis absorption spectra (a) and fluorescence emission spectra (d) of **Cy** in the D_2O, H_2O and H_2O containing various anions (concentration: 10 μM). UV-vis absorption spectra (b) and fluorescence emission spectra (e) of **Cy** in the D_2O, H_2O and H_2O containing different acid and base species (concentration: 10 μM). Absorption (c) and fluorescence (f) response of **Cy** in the presence of the other common species. 1, D_2O; 2, H_2O; 3, F^-; 4, Cl^-; 5, Br^-; 6, I^-; 7, CO_3^{2-}; 8, SO_4^{2-}; 9, HPO_4^{2-}; 10, KOH; 11, NaOH; 12, $CsCO_3$; 13, HCl; 14, H_2SO_4; 15, HNO_3; 16, Et_3N; 17, pyridine; 18, monoethanolamine; 19, sodium *tert*-butoxide; 20, CH_3COOH; 21, malonic; and 22, *p*-toluenesulfonic acid (λ_{ex} = 580 nm).

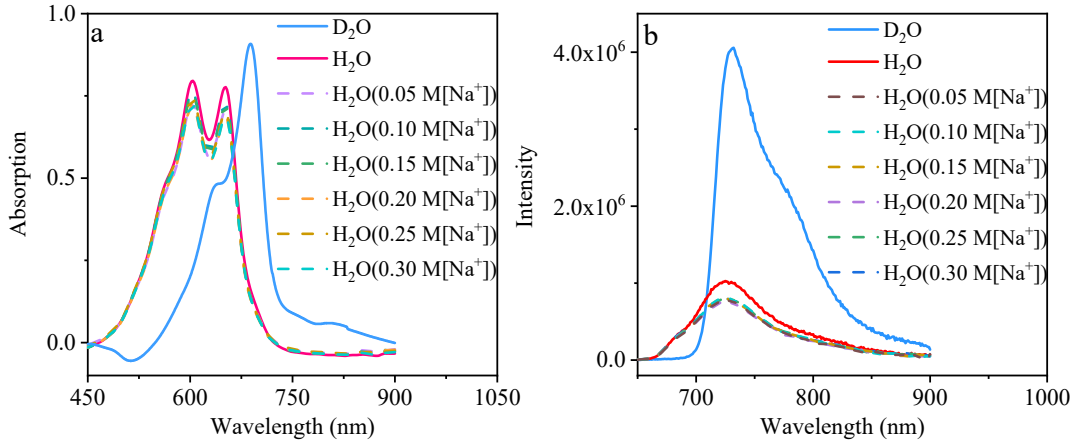

Fig. S11 UV-vis absorption spectra (a) and fluorescence emission spectra (b) of **Cy** in the D_2O, H_2O and H_2O with different concentration of Na^+ ion (λ_{ex} = 580 nm).

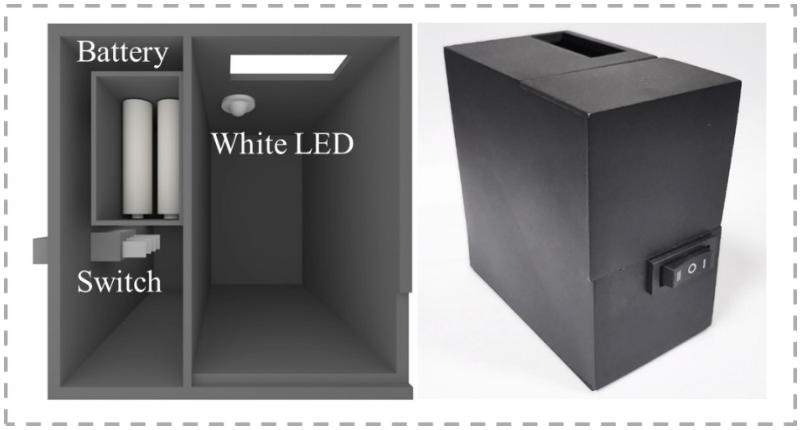

Scheme. S3 Schematic illustration of the basic construction of 3D-printed setup.

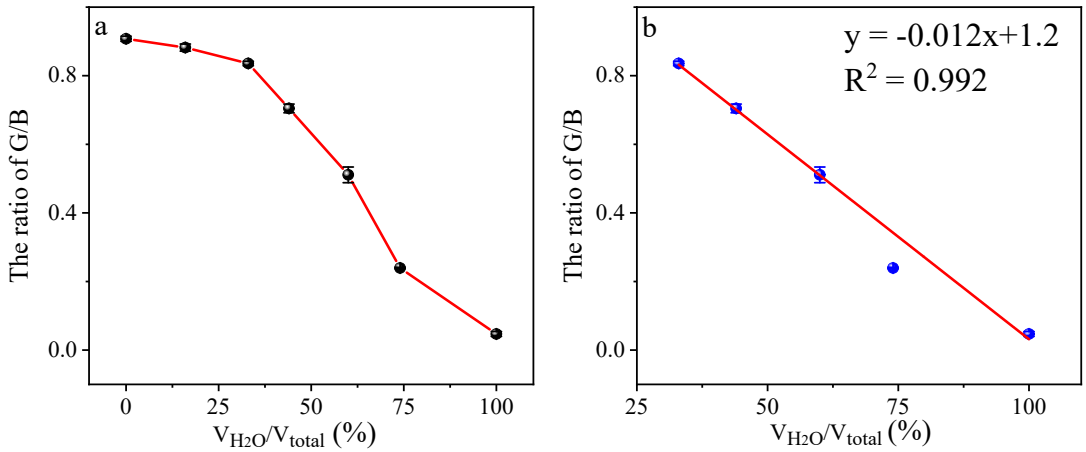

Fig. S12 (a) Calibration curve of the G/B ratio of corresponding solutions analyzed with a smartphone versus H_2O contents in H_2O-D_2O mixtures; and (b) linear relationship between the G/B ratio and the H_2O contents in H_2O-D_2O mixtures ranging from 33% to 100%.

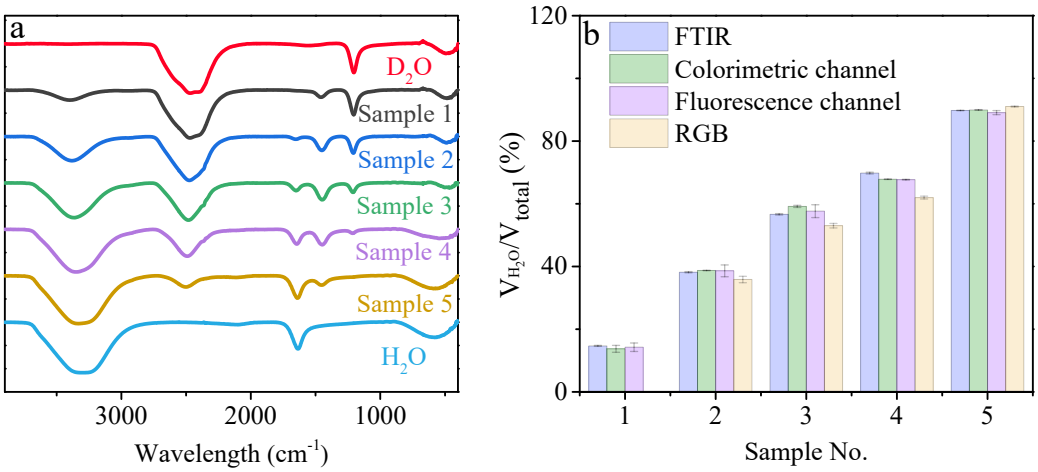

Fig. S13 (a) FTIR spectra of pure D_2O, pure H_2O and five samples prepared by random addition of H_2O into D_2O. (b) Determination of the H_2O content in H_2O-D_2O mixtures by the FTIR reference method and our proposed methods.

Table S3 Analytical results for the determination of H_2O content in total volume (%)

Sample no.	FTIR	Colorimetric channel	Fluorescence channel	RGB
1	14.7 ± 0.1	13.7 ± 1.1	14.3 ± 1.3	--[a]
2	38.2 ± 0.2	38.7 ± 0.1	38.6 ± 1.9	35.9 ± 1.0
3	56.7 ± 0.2	59.2 ± 0.3	57.7 ± 2.0	53.0 ± 0.7
4	69.8 ± 0.3	67.8 ± 0.1	67.7 ± 0.1	62.0 ± 0.4
5	89.8 ± 0.1	89.8 ± 0.1	89.1 ± 0.6	91.0 ± 0.1

[a] The ratio of G/B obtained by taking picture of this sample was not within the linear range, so the H_2O content calculation was not done.

Table S4. Comparison of currently reported organic small-molecule optical sensors based on the acid-base response mechanism for distinguishing between H_2O and D_2O.

Sensor[a]	Response	Solvent	LOD	Application	Ref
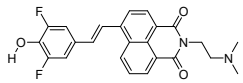 NIM-2F	Colorimetric Ratiometric	DMSO	0.24 vol%	--	2
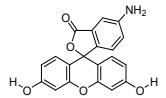 AF	Absorption and Fluorescence Dual Ratiometric	DMSO	0.08 vol%	--	2
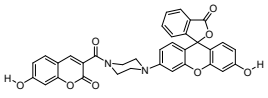 CF-D_2O	Fluorescence Turn-off	DMSO (10 μM 0.33 vol%)	0.165 vol%	--	3
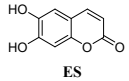 ES	Colorimetric Ratiometric and Fluorescence Turn-off	DMSO	--	--	4
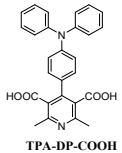 TPA-DP-COOH	Fluorescence Turn-off	H_2O	49.08 ppm 0.23 ppm	--	5
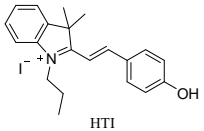 HTI	Absorption and Fluorescence Dual Ratiometric	DMSO (20 μM 0.2 vol%)	0.19 vol% (H_2O in D_2O) 0.59 vol% (D_2O in H_2O)	--	6

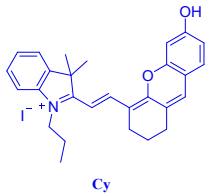 Cy	Absorption and Fluorescence Dual Ratiometric	DMF (100 μM 5 vol%)	0.061 vol% (H_2O in D_2O) 0.079 vol% (D_2O in H_2O)	RGB colorimetry	This work

[a] The full names of these sensors:

NIM-2F: (*E*)-6-(3,5-difluoro-4-hydroxystyryl)-2-(2-(dimethylamino)ethyl)-1H-benzo[de]isoquinoline-1,3(2H)-dione

AF: 5-amino-3',6'-dihydroxy-3H-spiro[isobenzofuran-1,9'-xanthen]-3-one

CF-D_2O: 3'-hydroxy-6'-(4-(7-hydroxy-2-oxo-2H-chromene-3-carbonyl)piperazin-1-yl)-3H-spiro[isobenzofuran-1,9'-xanthen]-3-one

ES: 6,7-dihydroxy-2H-chromen-2-one

TPA-DP-COOH: 4-(4-(diphenylamino)phenyl)-2,6-dimethylpyridine-3,5-dicarboxylic acid

HIT: (*E*)-2-(4-hydroxystyryl)-3,3-dimethyl-1-propyl-3H-indol-1-ium iodide

Table S5 Comparison of currently reported optical sensors based on other response mechanism for distinguishing between H_2O and D_2O.

Sensor Name	Type of system	Mechanism	Response	LOD	Ref
***p*-CPDs**	Carbon polymer dots	O-H oscillator quenching	Fluorescence Turn-off	0.10 vol %	[7]
Eu_1:Tb_5-PCM-22	MOF	O-H oscillator quenching	Ratiometric Fluorescence	--	[8]
SCU-UEu-1	MOF	O-H oscillator quenching	Ratiometric Fluorescence	1 vol%	[9]
Poly-Eu-2	MOF	O-H oscillator quenching	Fluorescence Turn-off	18.3 ppm	[10]
$\{[Tb(HL)(H_2O)_2]\cdot x(solv)\}_n$	MOF	O-H oscillator quenching	Ratiometric Fluorescence	0.48 vol %	[11]
PT10	Organic polymers	O-H oscillator quenching	Phosphorescence Turn-off	0.1 vol%	[12]
TCPP	Purely organic small molecules	O-H oscillator quenching	ultraviolet−visible, Fluorescence and electrochemiluminescence Turn-on	0.29 nM	[13]
Cy	Purely organic small molecules	Acid-base response	Absorption and Fluorescence Dual Ratiometric	0.061 vol% (H_2O in D_2O) 0.079 vol% (D_2O in H_2O)	This work

Table S6. The advantages and disadvantages of representative D_2O optical sensors.

Sensor	Advantages	Disadvantages
NIM-2F	naked-eye visualization, absorption ratiometric response	poor water-solubility, single channel response, insufficient detection sensitivity
AF	absorption/fluorescence dual-channel ratiometric response	poor water-solubility and naked-eye visualization, insufficient detection sensitivity
CF-D_2O	water-solubility, two turn-on fluorescence signals response	single channel response, poor naked-eye visualization, insufficient detection sensitivity
ES	readily available sensor, absorption/fluorescence dual-channel response,	poor water-solubility and naked-eye visualization
TPA-DP-COOH	brilliant water-solubility and sensitivity of detection	single channel response, poor naked-eye visualization
HIT	water-solubility, absorption/fluorescence dual-channel ratiometric response	insufficient naked-eye visualization and detection sensitivity
Cy	water-solubility, absorption/fluorescence dual-channel ratiometric response, naked-eye visualization	insufficient detection sensitivity

3. References:

1. L. Yuan, W. Lin, S. Zhao, W. Gao, B. Chen, L. He and S. Zhu, *J. Am. Chem. Soc.*, 2012, **134**, 13510-13523.
2. Y. Luo, C. Li, W. Zhu, X. Zheng, Y. Huang and Z. Lu, *Angew. Chem. Int. Ed.*, 2019, **58**, 6280-6284.
3. B. Dong, Y. Lu, W. Song, X. Kong, Y. Sun and W. Lin, *Chem. Commun.*, 2020, **56**, 1191-1194.
4. S. Gadiyaram, P. Kumar, A. Singh and D. Amilan Jose, *Microchem. J.*, 2022, **176**, 107244.
5. S. Zhang, Z. Li, B. Zhang, F. Dong, B. Han, J. Lv, Y. Sun, H. Lu, Y. Yang and H. Ma, *New J. Chem.*, 2021, **45**, 20441-20446.
6. J. Liu, X. Ma, Q. Song, J. Zang, J. Hao, W. Liu and J. Jiang, *Chem. Commun.*, 2022, **58**, 9262-9265.
7. J. Xia, Y. L. Yu and J. H. Wang, *Chem. Commun.*, 2019, **55**, 12467-12470.
8. S. G. Dunning, A. J. Nuñez, M. D. Moore, A. Steiner, V. M. Lynch, J. L. Sessler, B. J. Holliday and S. M. Humphrey, *Chem*, 2017, **2**, 579-589.
9. Y. Zhang, L. Chen, Z. Liu, W. Liu, M. Yuan, J. Shu, N. Wang, L. He, J. Zhang, J. Xie, X. Chen and J. Diwu, *ACS Appl. Mater. Interfaces.*, 2020, **12**, 16648-16654.
10. S. Zhang, W. Yin, Z. Yang, I. Shah, Y. Yang, Z. Li, S. Zhang, B. Zhang, Z. Lei and H. Ma, *Anal. Chem.*, 2020, **92**, 7808-7815.
11. M. Lei, F. Ge, X. Gao, Z. Shi and H. Zheng, *Inorg. Chem.*, 2021, **60**, 10513-10521.
12. Y. Lang, S. Wu, Q. Yang, Y. Luo, X. Jiang and P. Wu, *Anal. Chem.*, 2021, **93**, 9737-9743.
13. Z. Han, J. Wang, P. Du, J. Chen, S. Huo, H. Guo and X. Lu, *Anal. Chem.*, 2022, **94**, 8426-8432.